Superlattices and Microstructures 51 (2012) 886–892

Contents lists available at SciVerse ScienceDirect

Superlattices and Microstructures

journal homepage: www.elsevier.com/locate/superlattices

Effect of solution concentrations on crystal structure, surface topographies and photoluminescence properties of ZnO thin films

Jianguo Lv [a,b,c], Changlong Liu [b], Wanbing Gong [b], Zhenfa Zi [b], Xiaoshuang Chen [a,*], Kai Huang [d], Tao Wang [c], Gang He [c], Xueping Song [c], Zhaoqi Sun [c,*]

[a] National Laboratory for Infrared Physics, Shanghai Institute of Technical Physics, Chinese Academy of Sciences, Shanghai 200083, China
[b] School of Electronic and Information Engineering, Hefei Normal University, Hefei 230061, China
[c] School of Physics and Material Science, Anhui University, Hefei 230039, China
[d] Department of Mathematics & Physics, Anhui University of Architecture, Hefei 230601, China

ARTICLE INFO

Article history:
Received 15 December 2011
Received in revised form 14 February 2012
Accepted 16 February 2012
Available online 3 March 2012

Keyword:
ZnO thin films
Surface topographies
Hydrothermal
Photoluminescence

ABSTRACT

Zinc oxide thin films were deposited on silicon substrates via hydrothermal method. Microstructures, surface topographies and optical properties of ZnO thin films were systematically investigated by X-ray diffraction, atomic force microscopy and fluorescence spectrophotometer. The mean grain size and surface roughness of the thin films decrease first and then increase with increasing the concentration of zinc nitrate hexahydrate. The photoluminescence spectra of ZnO thin films, excited by the 240, 320, 360, 380 and 400 nm excitation wavelength, were investigated in detail. Based on our analysis, it can be noted that mechanisms of the ultraviolet, violet and blue emissions are attributed to the transitions from the localized levels below the conduction band, zinc vacancy, interstitial zinc and extended interstitial zinc levels to the valance band, respectively. Blue–violet emissions of ZnO have great potential in light emitting and biological fluorescence labeling applications.

© 2012 Elsevier Ltd. All rights reserved.

* Corresponding authors. Tel./fax: +86 21 25051403 (X. Chen), tel.: +86 551 5107284; fax: +86 551 5107237 (Z. Sun).
E-mail addresses: xschen@mail.sitp.ac.cn (X. Chen), szq@ahu.edu.cn (Z. Sun).

0749-6036/$ - see front matter © 2012 Elsevier Ltd. All rights reserved.
doi:10.1016/j.spmi.2012.02.014

www.sim.com.cn

1. Introduction

Recently great interest has been paid to wide band gap semiconductors due to the ever-increasing commercial desire for short wavelength lasers and blue light emitting diodes. ZnO is an attractive wide band gap (3.37 eV at room temperature) oxide semiconductor and has many potential applications such as in solar cells [1,2], transparent electrodes [3,4], blue/ ultraviolet (UV) light emitter device [5,6], gas sensor [7,8], surface electroacoustic wave devices [9], etc. These prospects have led to extensive studies of many aspects of ZnO nanostructures, including synthesis strategies, physical and chemical properties, and applications. Many different techniques such as magnetron sputtering [10,11], pulsed laser deposition [12,13], sol–gel method [14,15], molecular beam epitaxy [16], metal organic chemical vapor deposition [17], spray pyrolysis technique [18], electrospray [19] and hydrothermal growth method [20], have been employed to fabricate ZnO thin films. In spite of several decades of effort, some of the basic properties of ZnO were still not clear [21,22]. In particular, the origins of the defect-related emissions in the visible region have been controversial for quite a long time. Moreover, in the previous investigations, photoluminescence (PL) spectra were excited by specific wavelength of irradiating light. For Xe lamp excitation, the wavelength can be variable and this is an advantage to observe the PL spectra excited with different wavelengths.

In this letter, ZnO thin films were deposited on silicon substrates by means of hydrothermal growth method. The microstructure and surface topographies of the thin films were investigated and effects of excitation wavelengths on photoluminescence of the thin films were also studied. Photoluminescence mechanisms of the thin films were discussed in detail.

2. Experimental details

In our experiment, all reagents were of analytical grade and used without further purification. Silicon was used as substrates. ZnO seed was prepared by a sol–gel method. 8.76 g zinc acetate dehydrate ($Zn(CH_3COO)_2$ $2H_2O$) was dissolved into 80 mL ethylene glycol monomethyl ether at room temperature. Mono-ethanol amine (MEA) was used as the stabilizing agent. The molar ratio of MEA to zinc acetate dehydrate was kept as 1.0. They were mixed rapidly, and stirred at 60 °C for 120 min, then cooled to room temperature (RT). The solution served as the coating sol after being kept for one day. The sol was then spin coated on the substrate at 1500 rpm for 18 s, and 3000 rpm for 30 s. After spin coating, the substrates were heated at 150 °C for 10 min to remove the solvent and this procedure was repeated two times. These as-coated films were annealed at 600 °C for 60 min in air and then cooled down to RT. Growth of ZnO thin films was carried out by suspending the substrate in a 50 mL Teflon-lined stainless steel autoclave filled with 40 mL ethylene glycol monomethyl ether solution of zinc nitrate hexahydrate [$Zn(NO_3)_2$ $6H_2O$] and equimolar methenamine ($C_6H_{12}N_4$, HMT) at 95 °C for 6 h. The concentration of zinc nitrate hexahydrate was 0.02, 0.04, 0.06 and 0.08 mol/L, respectively. The molar ratio of HMT to zinc nitrate hexahydrate was kept as 1.0. Subsequently, the substrates were removed from the solution, rinsed with deionized water and dried in air at 60 °C.

The microstructure of the thin films was analyzed by a MACM18XHF X-ray diffractometer (XRD) with Cu Kα radiation source ($\lambda = 0.15405$ nm) and a scanning rate of 8°/min in the 2θ range of 30°–80°. The surface topographies were characterized by a CSPM4000 atomic force microscopy (AFM) by using contacting mode taken over a scale of 3 μm × 3 μm. The photoluminescence (PL) spectra were investigated with a F-4500 fluorescence spectrometer (FL) at RT. The wavelengths of excitation light were 240, 320, 360, 380 and 400 nm, respectively.

3. Results and discussion

XRD patterns of the ZnO thin films deposited on silicon substrates with different concentration of zinc nitrate hexahydrate are shown in Fig.1. The XRD patterns of the ZnO thin films indicate that they possess a polycrystalline hexagonal wurtzite crystal structure. Eight peaks appear at $2\theta = 31.77°$, 34.42°, 36.25°, 47.54°, 56.60°, 62.86°, 67.96° and 69.10°, which corresponds to (100), (002), (101), (102), (110), (103), (112) and (201) directions of the hexagonal ZnO structure, respectively. Based

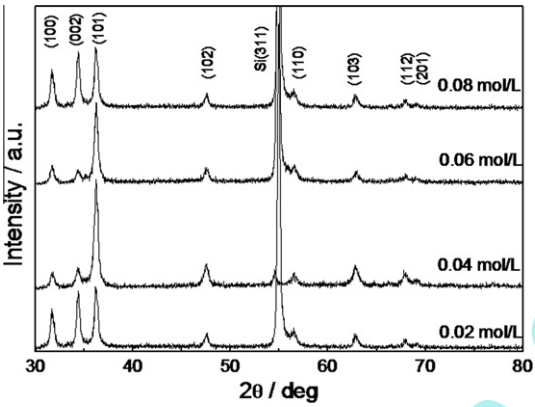

Fig. 1. X-ray diffraction patterns of the ZnO thin films.

on Fig. 1, it can be seen that the thin film obtained with a concentration of 0.02 mol/L zinc nitrate hexahydrate has random polycrystalline structure without preferred orientation. When the concentration increases to 0.04 and 0.06 mol/L, the intensity of the (1 0 1) peak is much stronger than that of other peaks in the XRD patterns, indicating that the thin films have a high (1 0 1) preferential orientation. However, when the concentration further increases to 0.08 mol/L, the thin film returns to random polycrystalline structure. From XRD patterns, the Si (3 1 1) peak has been demonstrated, which are attributed to the Si (1 0 0) substrate. As we know, the full width at half maxima (FWHM) of diffraction peak can be used to judge the crystal quality of ZnO thin films. As shown in Table 1, the FWHM of (1 0 1) diffraction peak increases first and then decreases, reaching a minimum of about 0.38° at 0.08 mol/L. The results indicate that ZnO thin film obtained with a concentration of 0.08 mol/L has the best crystal quality among all the ZnO thin films. The mean grain size (D) can be calculated by the following Scherrer formula [23]:

$$D = 0.9\lambda/\beta cos\theta \tag{1}$$

where λ, θ and β are X-ray wavelength (0.15405 nm), Bragg diffraction angle and FWHW of (1 0 1) peak, respectively. The mean grain sizes are 19.1, 17.6, 21.4 and 24.3 nm for the samples with 0.02, 0.04, 0.06 and 0.08 mol/L, respectively. This result indicates that the thin films are consisted of nanocrystalline grains. The minimum mean grain sizes may be attributed to secondary nucleation on the ZnO seeds as the concentration of zinc nitrate hexahydrate increases to 0.04 mol/L.

AFM images of the ZnO thin films with different concentration of zinc nitrate hexahydrate are shown in Fig.2. The root mean squares (rms) roughness values of the thin films grown at the 0.02, 0.04, 0.06, and 0.08 mol/L are 12.1, 11.0, 14.4, and 28.4 nm, respectively. The variation of rms roughness can be explained by the change of grain size of the ZnO thin films.

PL spectra of the ZnO thin films and its evolution as a function of concentration of zinc nitrate hexahydrate are shown in Fig. 3a. The PL spectra were excited by the 240 nm excitation wavelength. For the sample with 0.02 mol/L zinc nitrate hexahydrate, the spectrum exhibits a wide emission band in violet region with a UV shoulder at 382 nm and a weak emission band in green region. For the sample with 0.04 mol/L, the line is unchanged in shape, with a dominant UV emission at 396 nm and a

Table 1
Parameters of (1 0 1) diffraction peak of ZnO thin films.

(1 0 1) peak	0.02 mol/L	0.04 mol/L	0.06 mol/L	0.08 mol/L
FWHM (°)	0.45	0.50	0.42	0.38
D (nm)	19.1	17.6	21.4	24.3

www.sprn.com.cn

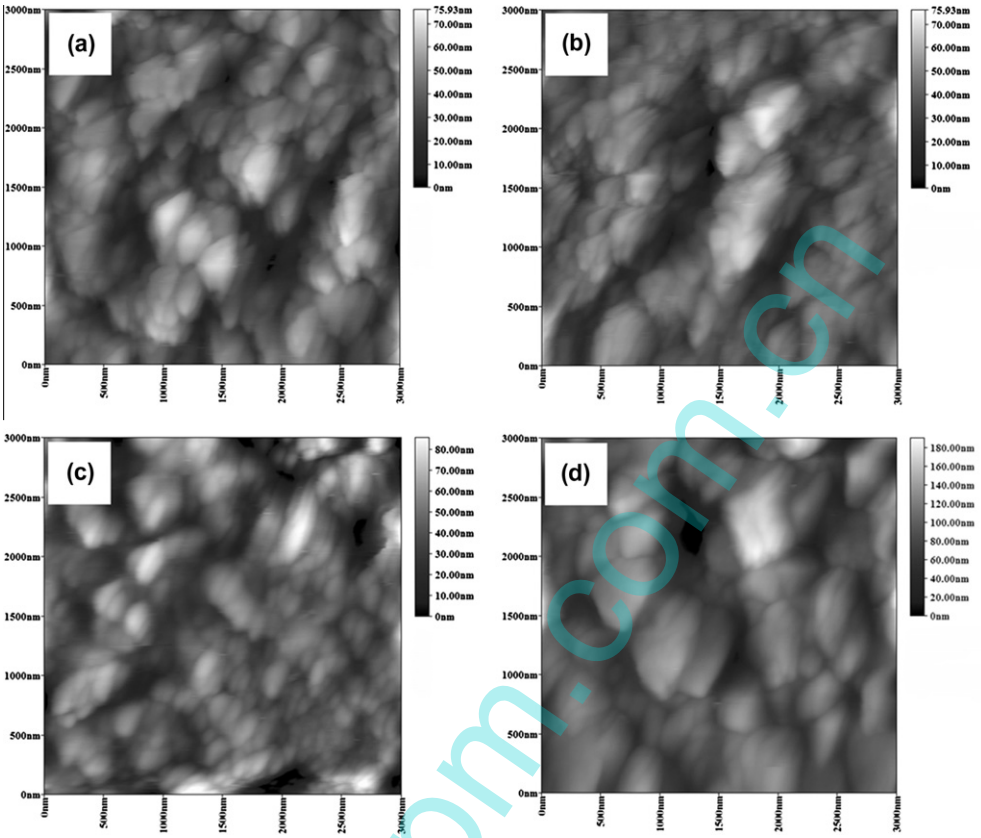

Fig. 2. AFM images of ZnO thin films with different concentrations of zinc nitrate hexahydrate: (a) 0.02 mol/L, (b) 0.04 mol/L, (c) 0.06 mol/L and (d) 0.08 mol/L.

weak deep-level emission in the green region. When the concentration increases to 0.06 mol/L, a wide emission band in the wavelength range 395–471 nm and a deep-level emission in the green region can be seen, as demonstrated in Fig. 3a. The intensity of the wide emission band changes seldom with increasing wavelength. For the sample with 0.08 mol/L, a 400–471 nm wide emission band and an emission band in green region can also be seen. However, the intensity of the emission band decreases with the increase of wavelength.

The PL spectra of ZnO thin films excited by the 320 and 360 nm excitation wavelength, are shown in Fig. 3b and c, respectively. For the sample with 0.02 mol/L, the violet emission centered at 415 nm down shifts to 411 nm and the UV shoulder at 382 nm disappears as the excitation wavelength increases from 320 nm to 360 nm. For the sample with 0.04 mol/L, the peak position remains changeless with increasing the excitation wavelength. When the concentration increases to 0.06 and 0.08 mol/L, a UV/violet emission band, a blue emission band and a weak green emission band have been observed. It can be seen that the ratio of the intensity of blue emission to that of violet emission decreases with the increase of excitation wavelength.

As shown in Fig. 3d and e, when the excitation energies are around (3.26 eV, 380 nm) and below (3.09 eV, 400 nm) the bandgap, a blue emission and a weak green emission can also be seen in the PL spectra. The intensity of blue emission increases and the peak position reduces slightly with decreasing the excitation energies. The origins of the defect-related deep-level emission have been investigated for a long time. The violet emission at 401 nm was attributed to the defects and/or lattice imperfections of the ZnO nanorods [24]. Wang et al. [25] believed that the violet emission (402 nm)

www.spm.com.cn

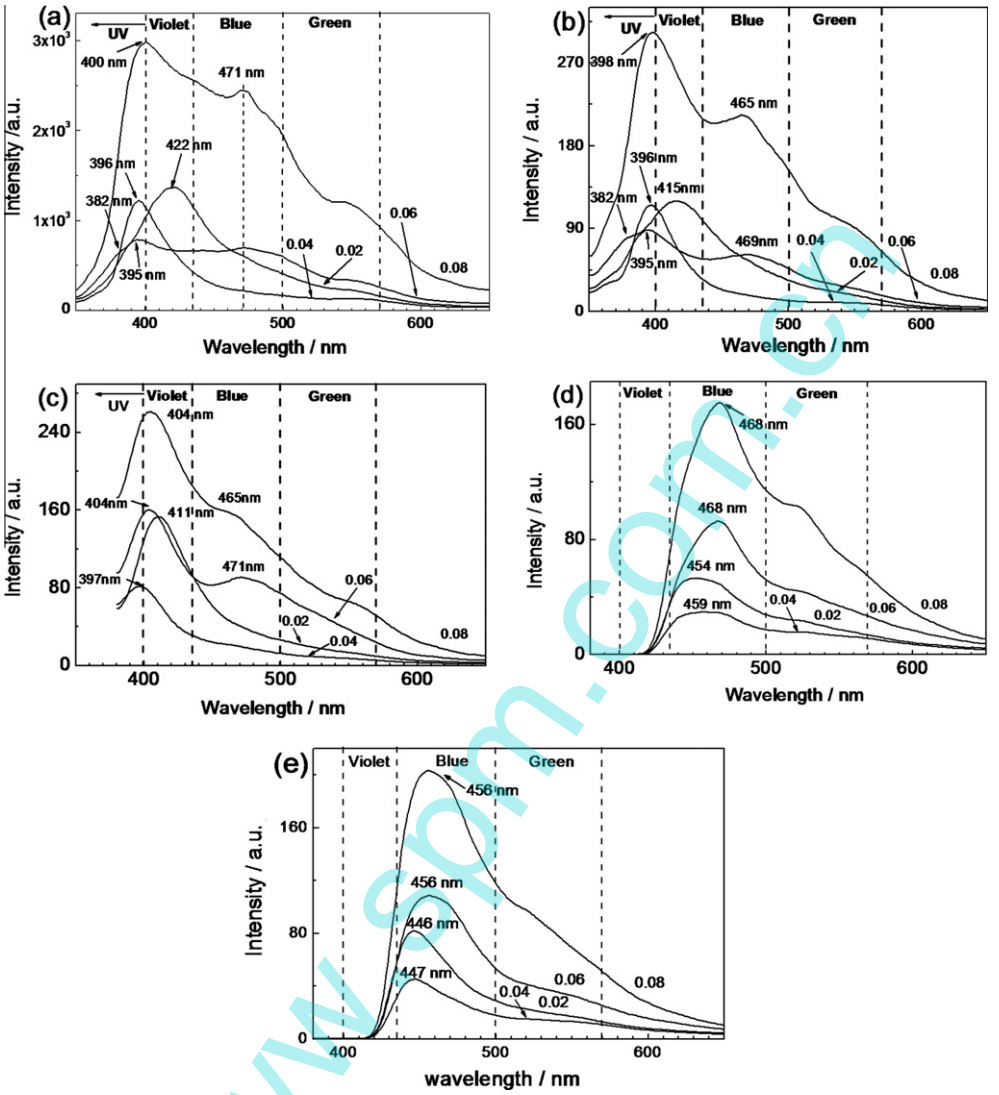

Fig. 3. Room temperature PL spectra of ZnO thin films excited by the 240 nm (a), 320 nm (b), 360 nm (c), 380 nm (d) and 400 nm (e) excitation wavelength with different concentrations.

was ascribed to the electron transition from the conduction band tail states to the valence band tail states. Gao et al. [26] thought that the UV emission located at 391 nm originated from the electron transition from the localized levels below the conduction band to the valance band. The formation of the localized levels was related to the breaking of lattice periodicity, originating from the free impurity atoms, various defects, surface and interface. Liang et al. [27] suggested that the origin of the violet emission at 415 nm (2.82 eV) could be due to the exciton recombination between the electrons in the conduction band and the holes localized at the zinc vacancy (V_{Zn}), and the origin of blue emission at 440 nm (2.99 eV) could come from the contribution of the exciton recombination between the electron localized at the interstitial zinc (Zn_i) and the holes in the valence band. The blue emission was observed by Zhang et al. [28,29] in the ZnO thin films at wavelength of 446 nm. They suggested that

www.spm.com.cn

the origin of the blue emission was due to the transition of electrons from the shallow donor level of the oxygen vacancies (V_O) to the valance band. Wang et al. [30] believed that the blue emission at 468 nm originated from the electron transition between the V_O and oxygen interstitial (O_i). Zeng et al. [31] reported that the blue emissions in the range of 455–488 nm could be due to the electron transition from extended Zn_i states, which were slightly below the simple Zn_i state, to the valance band. When $E_g \leqslant E_{ex}$ or $E_{Zni} \leqslant E_{ex} < E_g$, the electrons can first transit to the conduction band or Zn_i state, then relax to extended Zn_i states, and finally transit to the valance band with blue emission. It is well known that the origin of the green emission is due to the transition between singly ionized oxygen vacancies and photoexcited holes [32–34].

According to the above results about excited levels of UV, violet and blue emissions. Based on our analysis, it can be concluded that the origins of the UV, violet and blue emissions in our case are attributed to the electron transitions from the localized levels below the conduction band, V_{Zn}, Zn_i and extended Zn_i levels [31] to the valance band, respectively. For the sample with 0.02 mol/L zinc nitrate hexahydrate, when the excitation wavelength increases from 240 nm to 360 nm, the shift of violet emission comes from the competition of the transitions from V_{Zn} and Zn_i levels to the valance band. The UV shoulder at 382 nm may be attributed to the transition from the localized levels to the valance band. For the sample with 0.04 mol/L, the violet emissions $\sim$ 396 nm are assigned to the electron transition from localized levels below the conduction band to the valance band. For the sample with 0.06 and 0.08 mol/L, when the excitation wavelength is 240 nm, the electrons can first be excited up to the conduction band, then relax to localized levels, V_{Zn} level, Zn_i level and extended Zn_i levels, and finally transit to the valance band with a wide UV-violet-blue emission band. When the excitation wavelength increase up to 320 and 360 nm, the violet emission band and the blue emission band are attributed to the transitions from localized levels below the conduction band and extended Zn_i levels to the valance band.

For all the samples, blue-shifts in the blue emission peak has been observed with the increase in excitation wavelength from 380 to 400 nm. According to the origin, the electrons can first transit to the Zn_i level, then relax to extended Zn_i levels, and finally transit to the valance band [31].

4. Conclusions

In summary, ZnO thin films were deposited on silicon substrates covered by a thin ZnO seed via hydrothermal method. XRD and AFM measurements revealed that ZnO mean grain size, preferential orientation and surface roughness were affected by the concentration of zinc nitrate hexahydrate. A novel UV-violet-blue emission band were discovered in the ZnO thin films, which grown from solvent with 0.06 and 0.08 mol/L and excited by the 240 nm excitation wavelength. The UV-violet-blue emission band was assigned to the electrons transition from localized levels, V_{Zn} level, Zn_i levels and extended Zn_i levels to the valance band.

Acknowledgements

This work was supported by National Natural Science Foundation of China (Nos. 50872001, 51072001, 51102072, 51002156, 10804109), National Science Research Foundation for Scholars Return from Overseas, Ministry of Education of China, Natural Science Foundation of Anhui Higher Education Institution of China (Nos. KJ2010A284, KJ2010B172, KJ2010B024), Research Foundation of Hefei Normal University (Nos. 2010yj27, 2012kj17), and '211 Project' of Anhui University (No. KJTD004B).

References

[1] H. Ohta, K. Kawamura, M. Orita, M. Hirano, N. Sarukura, H. Hosono, Appl. Phys. Lett. 77 (2000) 475–477.
[2] K. Matsubara, P. Fons, K. Iwata, A. Yamada, K. Sakurai, H. Tampo, S. Niki, Thin Solid Films 431–432 (2003) 369–372.
[3] Y. Natsume, H. Sakata, Thin Solid Films 372 (2000) 30–36.
[4] G.K. Paul, S. Bandyapadhyay, S.K. Sen, Phys. Stat. Sol. A 191 (2002) 509–511.
[5] D.C. Look, D.C. Reynolds, C.W. Litton, R.L. Jones, D.B. Eason, G. Cantwell, Appl. Phys. Lett. 81 (2002) 1830–1832.
[6] X.Q. Wei, Z.G. Zhang, M. Liu, C.S. Chen, G. Sun, C.S. Xue, H.Z. Zhuang, B.Y. Man, Mater. Chem. Phys. 101 (2007) 285–290.

www.elsevier.com

[7] M.W. Ahn, K.S. Park, J.H. Heo, D.W. Kim, K.J. Choi, J.G. Park, Sens. Actuators B 138 (2009) 168–173.
[8] J. Yi, J.M. Lee, W.I. Park, Sens. Actuators B 155 (2011) 264–269.
[9] C.R. Gorla, N.W. Emanetoglu, S. Liang, W.E. Mayo, Y. Lu, M. Wraback, H. Shen, J. Appl. Phys. 85 (1999) 2595–2602.
[10] S. Mandal, R.K. Singha, A. Dhar, S.K. Ray, Mater. Res. Bull. 43 (2008) 244–250.
[11] C. Wang, Z. Chen, Y. He, L. Li, D. Zhang, Appl. Surf. Sci. 255 (2009) 6881–6887.
[12] X.M. Fan, J.S. Lian, Z.X. Guo, H.J. Lu, Appl. Surf. Sci. 239 (2005) 176–181.
[13] R.S. Ajimsha, R. Manoj, P.M. Aneesh, M.K. Jayaraj, Curr. Appl. Phys. 10 (2010) 693–697.
[14] N. Kumara, R. Kaurb, R.M. Mehra, J. Lumin. 126 (2007) 784–788.
[15] D. Wang, J. Zhou, G. Liu, J. Alloys. Compd. 487 (2009) 545–549.
[16] D.C. Oh, T. Suzuki, T. Hanada, T. Yao, J. Vac. Sci. Technol. B 24 (2006) 1595–1598.
[17] C.Y. Zhao, X.H. Wang, J.Y. Zhang, Z.G. Ju, C.X. Shan, B. Yao, D.X. Zhao, D.Z. Shen, X.W. Fan, Thin Solid Films 519 (2011) 1976–1979.
[18] N.L. Tarwal, V.V. Shinde, A.S. Kamble, P.R. Jadhav, D.S. Patil, V.B. Patil, P.S. Patil, Appl. Surf. Sci. 257 (2011) 10789–10794.
[19] A. Hosseinmardi, N. Shojaee, M. Keyanpour-Rad, T. Ebadzadeh, Ceram. Int. (2011) (In Press).
[20] K.H. Tam, C.K. Cheung, Y.H. Leung, A.B. Djurisic, C.C. Ling, C.D. Beling, S. Fung, W.M. Kwok, W.K. Chan, D.L. Phillips, L. Ding, W.K. Ge, J. Phys. Chem. B 110 (2006) 20865–20871.
[21] Ü. Özgör, Y. Alivov, C. Liu, A. Teke, M. Reshchikov, S. Dogan, V. Avrutin, S. Cho, H. Morkoc, J. Appl. Phys. 98 (2005). 041301–103..
[22] S.L. Mende, M.J.L. Driscoll, Mater. Today 10 (2007) 40–48.
[23] J.J. Ding, H.X. Chen, S.Y. Ma, Appl. Surf. Sci. 256 (2010) 4304–4309.
[24] X. Su, Z. Zhang, Y. Wang, M. Zhu, J. Phys. D 38 (2005) 3934–3937.
[25] Q.P. Wang, D.H. Zhang, Z.Y. Xue, X.T. Hao, Appl. Surf. Sci. 201 (2002) 123–128.
[26] X.D. Gao, X.M. Li, W.D. Yu, J. Solid State Chem. 177 (2004) 3830–3834.
[27] Z. Liang, X. Yu, B. Lei, P. Liu, W. Mai, J. Alloys Compd. 509 (2011) 5437–5440.
[28] D.H. Zhang, Z.Y. Xue, Q.P. Wang, J. Phys. D 35 (2002) 2837–2840.
[29] D.H. Zhang, Q.P. Wang, Z.Y. Xue, Appl. Surf. Sci. 207 (2003) 20–25.
[30] C. Wang, D. Xu, X. Xiao, Y. Zhang, D. Zhang, J. Mater. Sci. 42 (2007) 9795–9800.
[31] H.B. Zeng, G.T. Duan, Y. Li, S.K. Yang, X.X. Xu, W.P. Cai, Adv. Funct. Mater. 20 (2010) 561–572.
[32] K. Vanheusden, C.H. Seager, W.L. Warren, D.R. Tallant, J.A. Voigt, Appl. Phys. Lett. 68 (1996) 403–406.
[33] Y.W. Heo, M. Kaufman, K. Pruessner, D.P. Norton, F. Ren, M.F. Chisholm, P.H. Fleming, Solid-State Electron. 47 (2003) 2269–2273.
[34] L. Luo, L. Gong, Y.F. Liu, J. Chen, C.R. Ding, X.G. Tang, X.L. Li, Z.R. Qiu, H.Z. Wang, X.M. Chen, K.F. Li, H.H. Fan, K.W. Cheah, Opt. Mater. 32 (2010) 1066–1070.

www.spm.com.cn